

## Bi-Directional Relativistic Jets of the Radio Galaxy 1946+708: Constraints on the Hubble Constant

G. B. Taylor

NRAO, Socorro, NM 87801; gtaylor@nrao.edu

and

R. C. Vermeulen

NFRA, Dwingeloo, The Netherlands; rcv@nfra.nl

Astrophysical Journal Letters, in press

### ABSTRACT

We present measurements of bi-directional motions in the jets of the radio galaxy 1946+708 at  $z = 0.101$ . This is a Compact Symmetric Object with striking S-symmetry. Sensitive 15 GHz observations reveal a compact component at the center of symmetry with a strongly inverted spectrum, that we identify as the core. From five 4.9 GHz observations spread over 4 years we have determined the velocities of four compact jet components. If simple kinematic models can be applied then the inclination of the source and the bulk jet velocity can be directly determined for any assumed value of the Hubble constant. Conversely, the measurements already place constraints on the Hubble constant, and we show how further observations of 1946+708 can yield an increasingly accurate determination of  $H_0$ .

*Subject headings:* distance scale — galaxies: active — galaxies: individual (1946+708)  
— galaxies: jets — radio continuum: galaxies

## 1. Introduction

A direct measure of the distance to an object can be obtained by observing (angular) motion in it, if the intrinsic (linear) velocity can be ascertained independently. Lynden-Bell (1977) first suggested that Hubble’s constant could be determined from observations of superluminal extragalactic radio sources. While he assumed a light-echo model, the idea can be generalized to the now commonly accepted relativistic jet model (e.g. Marscher & Broderick 1982). Here, we will make use of the additional constraints obtained by observing relativistic motion of a pair of knots in anti-parallel jets; we believe this is the first such detection in an AGN.

The radio source 1946+708 is identified with an  $m_v = 18$  galaxy at a redshift  $z = 0.101$  (Stickel & Kühr 1993). This source is one of a family of Compact Symmetric Objects (CSOs) comprising  $\sim 5\%$  of sources in complete flux limited samples selected at high frequencies (Readhead et al. 1996; Taylor et al. 1996a). The CSOs are defined as sources less than 1 kpc in size having radio emission on both sides of the central engine that is thought to be relatively free of beaming effects (Wilkinson et al. 1994). Nearly all CSOs have two steep-spectrum hot-spots and/or lobes and most have an inverted or flat-spectrum core (Taylor et al. 1996a). Preliminary measurements of the jet motions based on the first two epochs at 5 GHz were discussed by Taylor, Vermeulen, & Pearson (1995).

## 2. Observations and Data Reduction

The first VLBI observation of 1946+708 was made on 1992 Sep 24 using multiple snapshots with a global array of 15 antennas at 4.9 GHz (Taylor et al. 1994). The second epoch observation was made on 1994 Sep 15 in a similar fashion, although with only 12 antennas. The telescopes used include those in the European VLBI Network, the Very Long Baseline Array (VLBA) operated by NRAO<sup>1</sup>, the Very Large Array<sup>1</sup>, the NRAO 140-foot<sup>1</sup> and the Haystack Observatory. Three further 4.9 GHz epochs were taken using the VLBA, at epochs 1995 Mar 22, 1995 Sep 03, and 1996 Aug 18. In addition we also present 8.4 and 15 GHz VLBA observations made on 1996 July 7. The calibration, fringe-fitting, and mapping was performed following the procedures described by Taylor et al. (1994).

In Fig. 1 we show nearly contemporaneous observations at 5, 8 and 15 GHz; the 8 GHz image has the greatest sensitivity. Model-fitting of Gaussian components to the self-calibrated visibility data was performed on each 5 GHz epoch using Difmap (Shepherd, Pearson & Taylor 1994, 1995). The shapes of the components were fixed after fitting to the first epoch, and in subsequent epochs each component was allowed only to move, and to vary in flux density in order to fit the independently self-calibrated visibility data. The reduced  $\chi^2$  of the fit between the model and

---

<sup>1</sup>The National Radio Astronomy Observatory is operated by Associated Universities, Inc., under cooperative agreement with the National Science Foundation

data is 1.06, 1.04, 0.94, 1.07, and 0.97 for epochs 1–5 respectively. The errors in the component positions were determined as the shifts that result in a significant (2%) increase in the reduced  $\chi^2$  of the fit after all other components had been allowed to reconverge.

### 3. Discussion

#### 3.1. Location of the core and hot spots

In Fig. 2 we plot the integrated spectrum of 1946+708, from measurements using the VLA and the Owens-Valley millimeter array. Also shown are the individual spectra of components C (inverted) and NHS (steep), from our VLBA observations and a 1.3 GHz VLBA observation by Conway & Taylor (1997). The striking S-symmetry (Fig. 1) strongly reinforces the idea that the centrally located compact inverted spectrum component, C, is the center of activity. We further believe that the outer components NHS and SHS are genuine terminal hot spots; a 21 cm VLA image shows 1946+708 to be unresolved in a  $1.7''$  beam with no extended component stronger than 0.11 mJy/beam (Taylor et al. 1996b).

We measure a formally insignificant expansion rate between the two hot spots of  $0.22 \pm 0.3$  mas/yr. We have also measured the separation rate between the strong northern hot spot and the core at 15 GHz to be  $0.03 \pm 0.03$  mas in 1.29 years. This latter measurement gives a  $3\sigma$  upper limit on the advance speed of the northern hot spot of  $< 0.4h^{-1}c$ , and implies an age for the source of  $> 200$  years.

Unfortunately, the core component is too weak in the 5 GHz images to use as a reference in aligning the epochs. Therefore, we have used the strong northern hotspot as the reference. Our conclusion, below, of the existence of bi-directional motion in the jets is not critically dependent on this choice and can be avoided only by assuming that the core is somewhere in the southern part of the source (for example, if S2 were stationary), but this would require a significant velocity for the northern hot spot (NHS) and a jet component (C) with bizarre properties – both of which seem unlikely. The positions of all components are plotted with respect to the midpoint between the hot spots. This midpoint is  $< 0.2$  mas from the intersection point of the line connecting N5 and S5 with the line connecting N2 and S2, and is  $< 0.3$  mas from the core component visible in the 15 GHz image (Fig. 1).

The trajectories of the two best defined pairs, N2/S2 and N5/S5, are shown in Fig. 3. To within the measurement errors these trajectories can be fit with a straight line on the sky. In Fig. 4 we show the motion of each component projected along the fitted trajectories. The slope of this line corresponds to the velocity of the component. Based on these observations no acceleration or deceleration of components is required.

### 3.2. Kinematics in 1946+708; Constraints on the Hubble Constant

For simultaneously ejected components moving in opposite directions at an angle  $\theta$  to the line of sight at a velocity  $\beta$ , it follows directly from the light travel time difference that the ratio of apparent projected distances from the origin ( $d_a$  for the approaching side,  $d_r$  for the receding side) as well as the ratio of apparent motions (approaching:  $\mu_a$ , receding:  $\mu_r$ ) is given at any time by

$$\frac{\mu_a}{\mu_r} = \frac{d_a}{d_r} = \left( \frac{1 + \beta \cos \theta}{1 - \beta \cos \theta} \right). \quad (1)$$

There is a similar relationship for the ratio between the flux density on the approaching side,  $S_a$  to that on the receding side,  $S_r$ , after including the effects of Doppler beaming:

$$\frac{S_a}{S_r} = \left( \frac{1 + \beta \cos \theta}{1 - \beta \cos \theta} \right)^{k-\alpha}, \quad (2)$$

where  $\alpha$  is the spectral index ( $S \propto \nu^\alpha$ ), and  $k = 2$  for a continuous jet or  $k = 3$  for discrete jet components (but see e.g. Lind & Blandford 1985).

We can apply the above equations to derive the product  $\beta \cos \theta$  in 1946+708, assuming that C is the core and that pairs of identical components N5/S5 and N2/S2 were ejected simultaneously. Components N5/S5 are still rather close to the core, and there is evidence for systematic position errors due to blending of the features, so we will not yet analyze N5/S5. Using the proper motion ratio  $\mu_{N2}/\mu_{S2} = 2.2 \pm 0.9$  yields  $\beta \cos \theta = 0.38 \pm 0.13$ . However, this derivation is subject to substantial additional systematic errors due to the uncertainty in pinpointing the stationary reference point. The flux density ratio  $S_{N2}/S_{S2} = 1.86 \pm 0.11$  indicates  $\beta \cos \theta = 0.09 \pm 0.03$ , for  $k = 3$ , and  $\beta \cos \theta = 0.12 \pm 0.03$ , for  $k = 2$ , with a spectral index of  $\alpha = -0.6$ , estimated from the multi-frequency images. This is subject of course to the further assumption that the emitted fluxes are still identical, and it is somewhat remarkable that the result is close to what we believe to be the most accurate estimate,  $\beta \cos \theta = 0.16 \pm 0.01$ , which follows from  $d_{N2}/d_{S2} = 1.38 \pm 0.03$ . We plot this constraint on Figure 5.

Another constraint on the two parameters  $\beta$  and  $\theta$  can be obtained from the separation rate  $\mu_{sep} = |\mu_a| + |\mu_r|$ , which, unlike  $\mu_a/\mu_r$ , is not subject to the uncertainty in the reference point. From geometry and the conversion of angular to linear velocity we have:

$$v_{sep} = \mu_{sep} D_a (1 + z) = \frac{2\beta c \sin \theta}{(1 - \beta^2 \cos^2 \theta)}, \quad (3)$$

where  $v_{sep}$  is the projected separation velocity,  $D_a$  is the angular size distance to the source, and  $z$  is the redshift. We will take  $q_0 = 0.5$  in Friedmann cosmology; this choice is unimportant given the low redshift  $z = 0.101$  of 1946+708. We measure  $\mu_{sepN2-S2} = 0.17 \pm 0.028$  mas/yr which gives  $v_{sepN2-S2} = (0.74 \pm 0.12) h^{-1} c$ , with  $H_0 = 100h$  km s<sup>-1</sup> Mpc<sup>-1</sup>. The resultant locus of  $\beta$  and  $\theta$  is illustrated in Figure 5 for two choices:  $h = 1$  and  $h = 0.37$ .

For  $h = 1$ , the intersection with  $\beta \cos \theta$  is already at a substantial angle to the line-of-sight ( $\theta \sim 65^\circ$ ) and a moderate value of  $\beta \sim 0.4$ . Smaller angles and smaller jet velocities (limit:  $\beta \geq 0.15$  because  $\theta \geq 0^\circ$ ) would need an implausibly high Hubble constant. On the other hand, the fact that  $\beta < 1$  not only gives the weak limit  $\theta < 81^\circ$ , but also implies that  $h > 0.37$  ! The  $\beta \cos \theta$  area in Fig 5 is nearly vertical for all plausible values of  $H_0$ , meaning that  $\theta$  is constrained to the narrow range  $65\text{--}80^\circ$ , while the allowed values of  $\beta$  and  $h$  are roughly inversely proportional. Thus, for relativistic jets with  $\beta \geq 0.9$ , as are frequently assumed to exist in high luminosity AGN, values of  $H_0$  towards the lower end of the commonly discussed range are much more plausible than high values.

There are several additional methods which can in principle be used to further constrain the jet Doppler factor or velocity, and hence improve our determination of  $H_0$ . These are: (1) flux density variability studies (Rees 1967); (2) comparison of predicted and observed inverse Compton X-ray emission (Marscher & Broderick 1982); (3) measurement of relativistic aberration (Unwin & Wehrle 1992); and (4) measurements of equipartition Doppler factors (Readhead 1994). The various parameters involved scale with  $H_0$  to different powers, effectively leading to different curves in a diagram like Figure 5. Thus, a combination of more methods can improve the determination of  $H_0$ , and we plan to pursue all of them.

### 3.3. Evolution of the Jet Components

Assuming that the components N2 and S2 were ejected at the same time and have kept a constant velocity, their age at the time of the first epoch observations was 93 years, implying ejection in 1899. The age of N5 and S5 would be 8 years, with an ejection date of 1984. At  $\theta \geq 65^\circ$ , the observed flux densities of the jet components in 1946+708 are only mildly Doppler boosted. Therefore they have a greater intrinsic surface brightness than the jets found in larger radio galaxies or even in typical parsec-scale core-jet sources (Taylor et al. 1994).

The source shows significant curvature, and at  $\theta \geq 65^\circ$  this must be largely intrinsic. If the components are indeed moving on curved tracks we expect a discrepancy between the geometry derived from the distance ratio  $d_a/d_r$ , which depends on the time-integral angle since ejection, and the motion ratio  $\mu_a/\mu_r$ , which reflects the angle only during the monitoring interval. There is some suggestion from our analysis above that knots N2 and S2 might indeed be in the process of curving into and away from the line of sight, respectively. On the other hand, the current monitoring series does not rule out that the knots might be moving ballistically. In that case, one might attribute the overall curvature to precession of the central engine. The current data do not warrant fitting of a model, but the precession period would be quite short (<200 years), much less than expected for a stable binary black hole in the model proposed by Begelman, Blandford & Rees (1980). Prolonged astrometric monitoring will surely be very illuminating.

#### 4. Conclusions

Components in the parsec-scale jet and counterjet in 1946+708 are observed to move away from the center of activity. Pairing components up under the assumption of simultaneous ejections gives reasonable agreement between arm length, flux density, and velocity ratios. These relations also allow us to constrain Hubble's constant to  $H_0 \geq 37$ . Future measurements, especially those carried out at higher frequencies, will further elucidate the source geometry and improve in accuracy the constraints on the motions and thus on the Hubble constant linearly with time. We are also in the process of examining other CSOs for bi-directional motions. If enough of these twin-jet systems can be found over a range in redshift then they might eventually provide a direct determination of  $q_0$  as well.

We thank Tim Pearson for his encouragement and involvement in the early stages of this work. We are grateful to an anonymous referee for helpful comments. We thank the staffs at the observatories and the staff of the JPL/Caltech Block II Correlator and the VLBA Correlator for their assistance. This work was supported in part by the NSF under grants AST-9117100 and AST-9420018.

#### REFERENCES

- Begelman, M. C., Blandford, R. D., & Rees, M. J. 1980, *Nature*, 287, 307
- Conway, J. E., & Taylor, G. B. 1997 in preparation
- Lind, K. R., & Blandford, R. D. 1985, *ApJ*, 295, 358
- Lynden-Bell, D. 1977, *Nature*, 270, 396
- Marscher, A. P., & Broderick, J. J. 1982, in *IAU Symposium No. 97: Extragalactic Radio Sources* eds. D. S. Heeschen & C. M. Wade (Dordrecht:Reidel), p. 359
- Readhead, A. C. S. 1994, *ApJ*, 426, 51
- Readhead, A. C. S., Taylor, G. B., Xu, W., Pearson, T. J., Wilkinson, P. N., & Polatidis, A. G. 1996, *ApJ*, 460, 612
- Rees, M. J. 1967, *MNRAS*, 135, 345
- Shepherd, M. C., Pearson, T. J., & Taylor, G. B. 1994, *BAAS*, 26, 987
- Shepherd, M. C., Pearson, T. J., & Taylor, G. B. 1995, *BAAS*, 27, 903
- Stickel, M., & Kühr, H. 1993, *A&AS*, 100, 395
- Taylor, G. B., Vermeulen, R. C., Pearson, T. J., Readhead, A. C. S., Henstock, D. R., Browne, I. W. A., & Wilkinson, P. N. 1994, *ApJS*, 95, 345
- Taylor, G. B., Vermeulen, R. C., & Pearson, T. J. 1995, in *Quasars and AGN: High Resolution Radio Imaging*, Proc. Natl. A. Sci., 92, 11381

Taylor, G. B., Readhead, A. C. S., & Pearson, T. J. 1996a, *ApJ*, 463, 95

Taylor, G. B., Vermeulen, R. C., Readhead, A. C. S., Pearson, T. J., Henstock, D. R., & Wilkinson, P. N. 1996b, *ApJS*, 107, 37

Unwin, S. C., & Wehrle, A. E. 1992, *ApJ*, 398, 74

Wilkinson, P. N., Polatidis, A. G., Readhead, A. C. S., Xu, W., & Pearson, T. J. 1994, *ApJ*, 432, L87

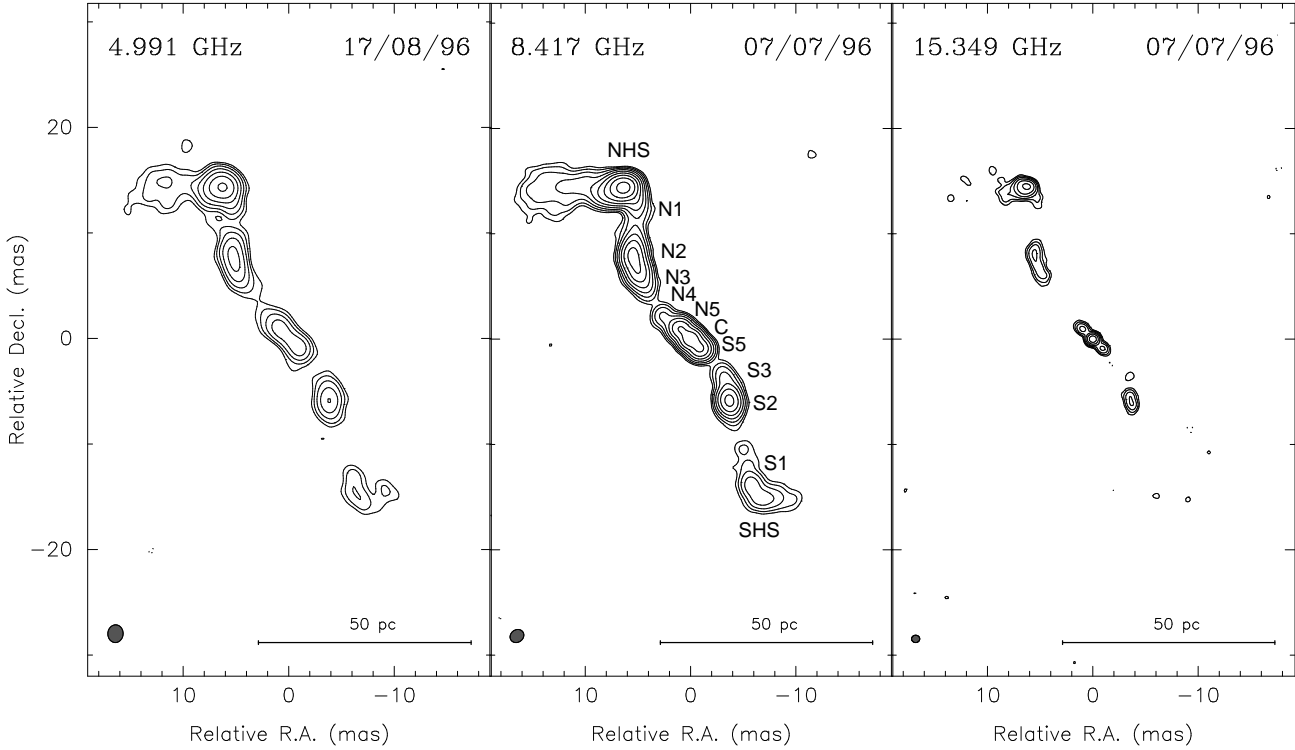


Fig. 1.— Nearly contemporaneous VLBA observations of 1946+708 at 5, 8 and 15 GHz. The synthesized beam is drawn in the lower left-hand corner of each plot and has dimensions:  $1.68 \times 1.45$  mas in position angle  $-3.4^\circ$  at 5 GHz;  $1.37 \times 1.18$  mas in position angle  $-55^\circ$  at 8 GHz; and  $0.78 \times 0.7$  mas in position angle  $90^\circ$  at 15 GHz. Contours are drawn logarithmically at factor 2 intervals with the first contour at 2, 0.25, and 0.75 mJy/beam at 5, 8 and 15 GHz respectively. The components labeled NHS and SHS in the 8 GHz image are the northern and southern hot spots respectively. The component labeled “C” we identify as the core.



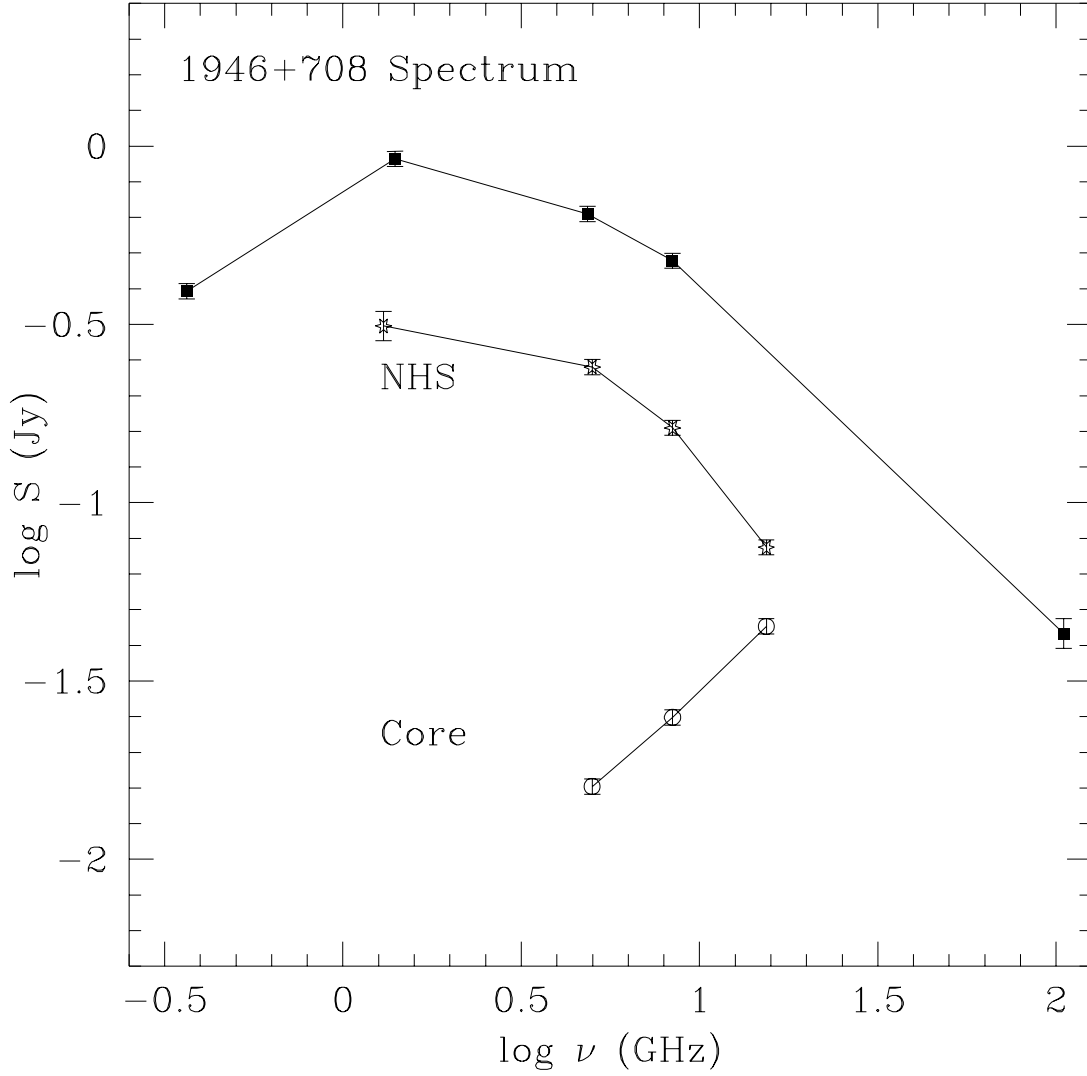


Fig. 2.— The spectrum of 1946+708. Total flux densities (at various epochs, from Taylor et al. 1996b) are shown plotted as filled squares. Flux densities for the northern hot spot (stars) and core component (circles) have been derived from modelfits to the VLBA 1996 epoch data except for the 1.3 GHz measurement which comes from VLBA data at epoch 1995 Mar 22 as described in Conway & Taylor (1997).

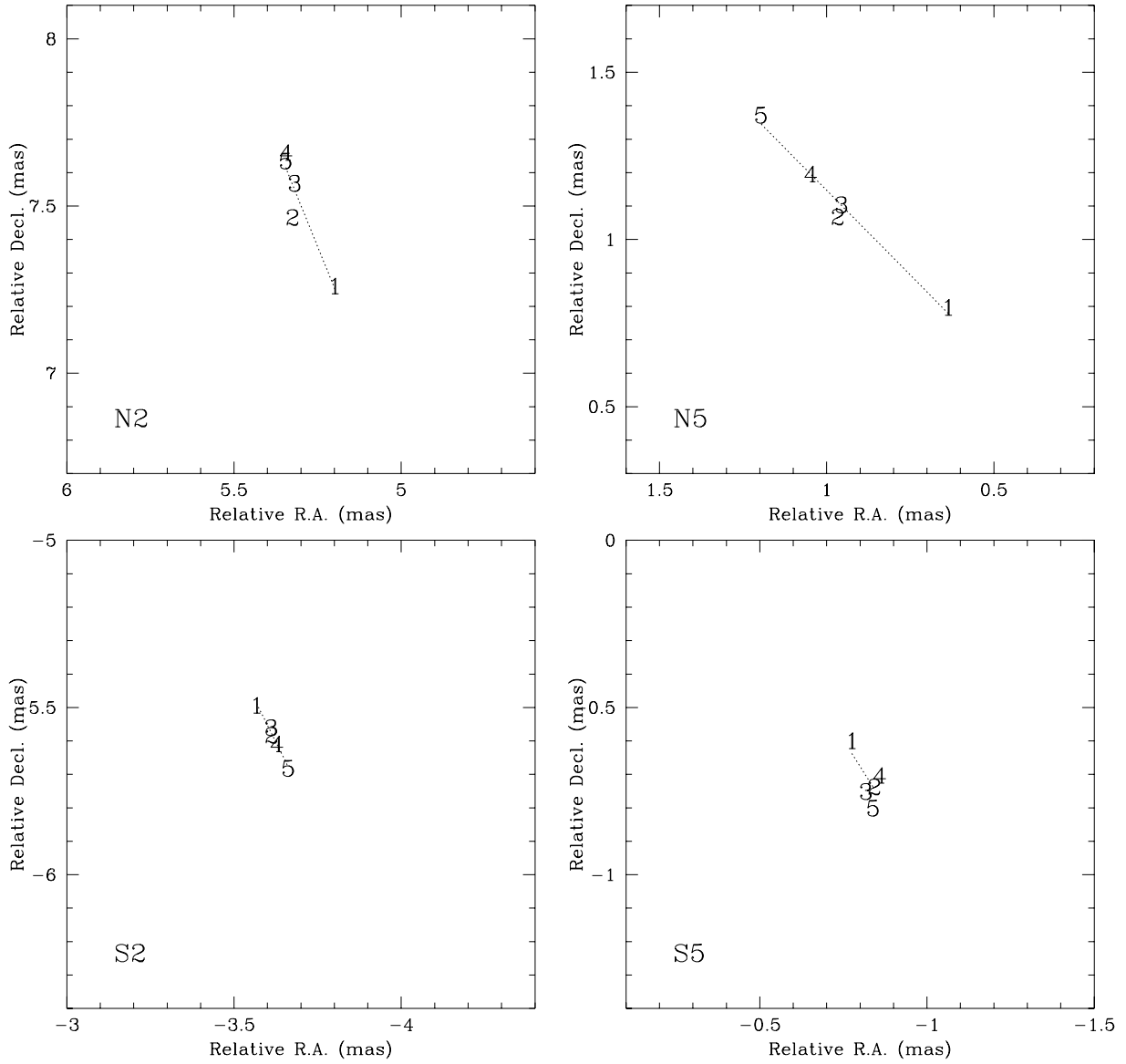


Fig. 3.— Positions of the components N2, S2, N5 and S5 relative to the source center. The best-fit straight-line motions are shown as a dotted line. The numbers correspond to the position of the component at epochs 1 = 1992 Sep 24, 2 = 1994 Sep 15, 3 = 1995 Mar 22, 4 = 1995 Sep 3, and 5 = 1996 Aug 18.

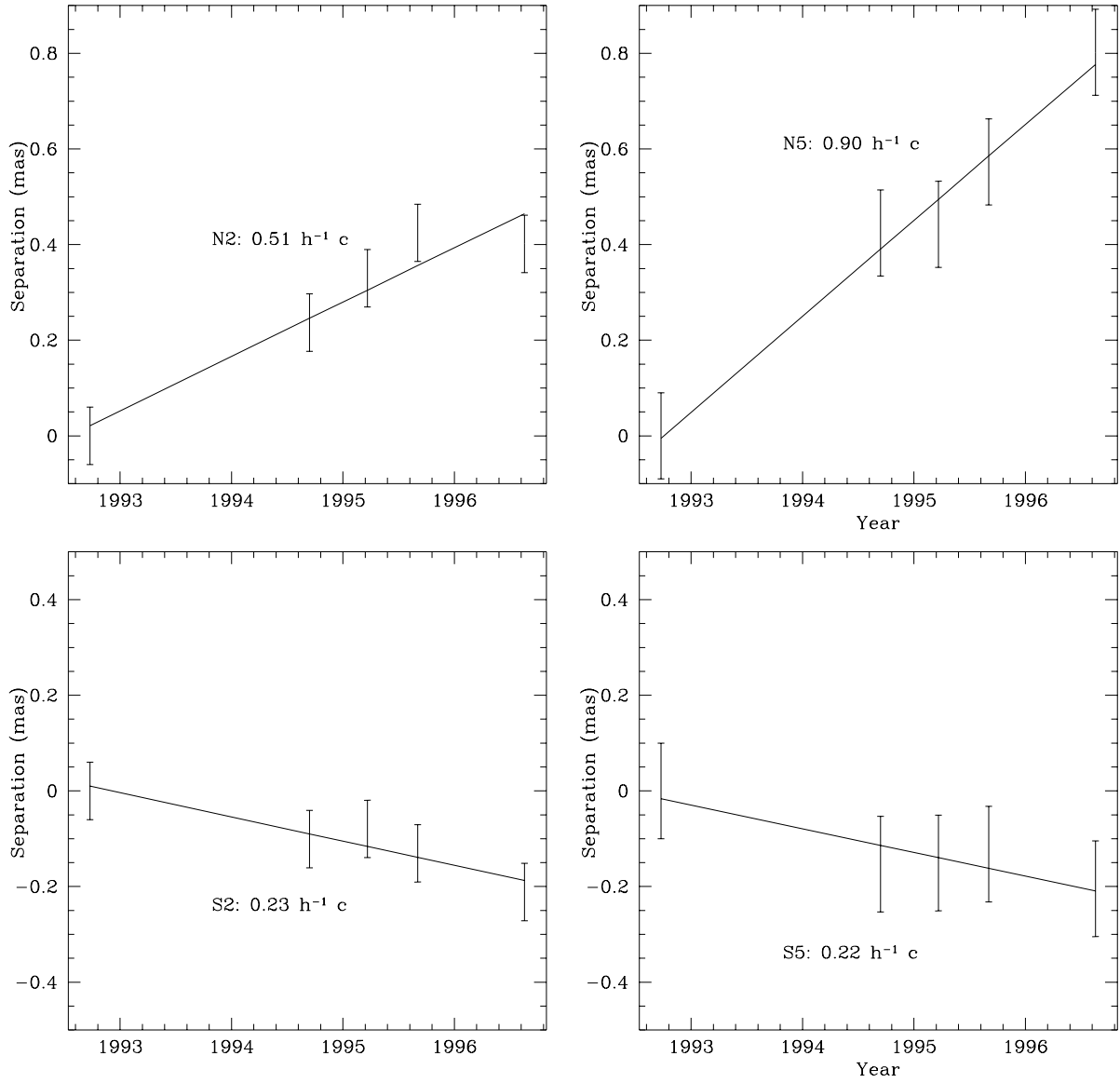


Fig. 4.— Velocities of the components N2, S2, N5 and S5 fitted to the projected positions along the straight line which best fits the measured positions (see Fig. 3). The zero point is taken to be the position of the component at the first epoch. The southern components are plotted with negative separations to reflect their near  $180^\circ$  difference in direction.

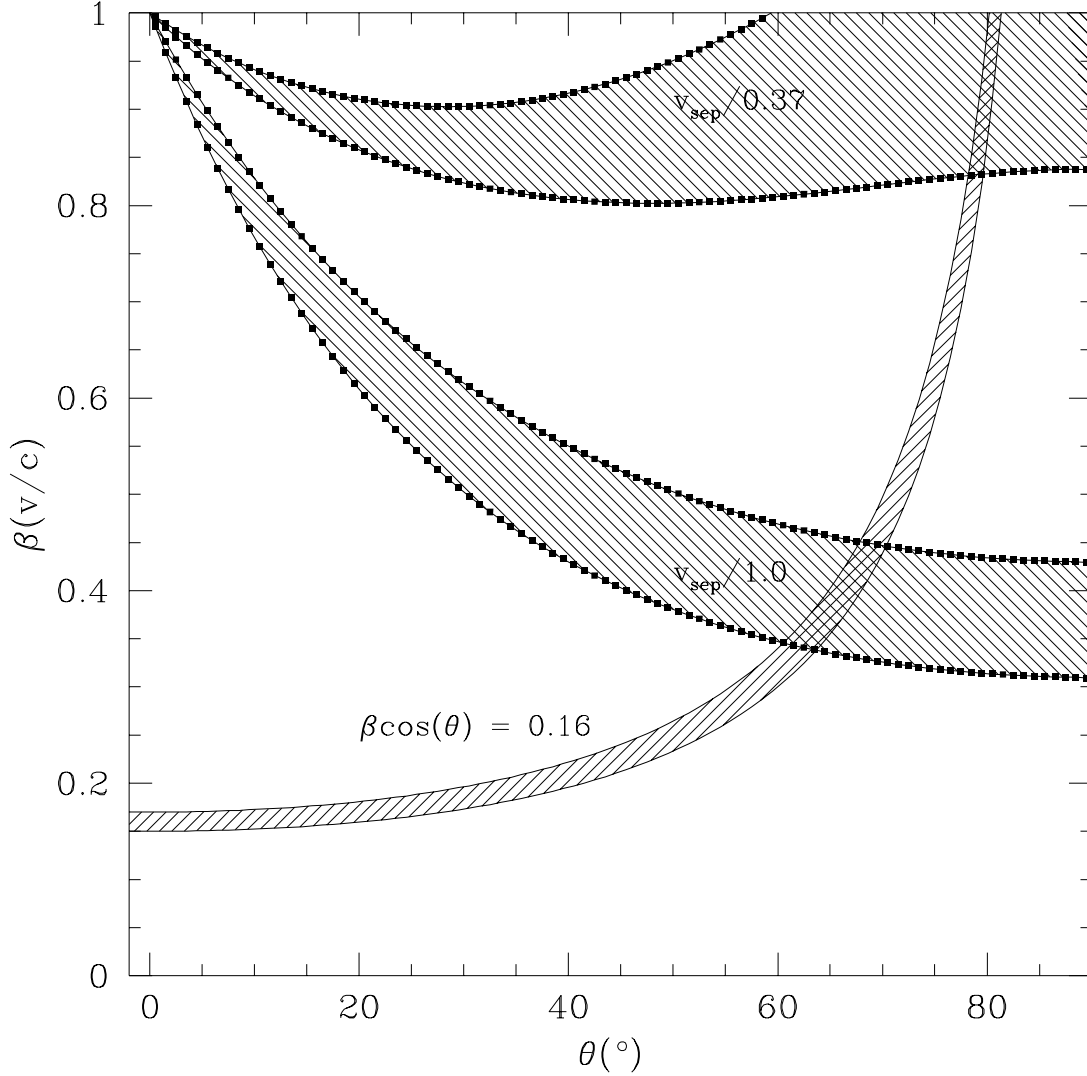


Fig. 5.— The jet velocity ( $\beta$ ) plotted against the inclination of the source ( $\theta$ ) measured from the line-of-sight to the jet axis. The solid lines represent the constraint  $\beta \cos \theta = 0.16 \pm 0.01$  from the arm-length ratio of components N2 and S2 (Eq. 1). The heavy dashed lines show the constraint from the observed separation velocity,  $h^{-1}v_{sep}$ , for N2 and S2 with  $h = 0.37 \pm 0.06$ , and  $1.0 \pm 0.16$  where  $h = H_0/100 \text{ km s}^{-1} \text{ Mpc}^{-1}$  (Eq. 3). If  $\beta = 1$  then  $h = 0.37 \pm 0.06$  where the uncertainty in  $h$  stems from uncertainty in the measurement of  $v_{sep}$ .